Local Time and Seasonal Variations in the D-Region Ionosphere: Does It Reflect Sudden Stratospheric Warming Effects?

Yuma Nozaki, Hiroyo Ohya, Fuminori Tsuchiya, Kenro Nozaki, Hiroyuki Nakata, and Kazuo Shiokawa

Abstract – This article presents local time (LT) and seasonal variations in the D-region ionosphere using low-frequency (LF, 30 kHz to 300 kHz) transmitter signals of the JJY (60 kHz)-Rikubetsu path over Japan. We show the variations in amplitude (ΔA) and phase (ΔP) of the LF transmitter signal from the mean value throughout 2017. In daytime at 09:00 LT to 15:00 LT, both ΔA and ΔP were larger than other LT. ΔA was large in summer and winter, while ΔP was large in spring and fall. These observations were compared with calculations based on the wave-hop method. The difference in results between observation and calculation would be due to neutral wind effects. In January 2017, both ΔA and ΔP were large, which could be caused by neutral winds associated with sudden stratospheric warming.

1. Introduction

Electron density in the D-region ionosphere varies, depending on solar zenith angle and solar activity, which are functions of local time (LT), season, and solar cycle. In addition to regular variations, solar flares, geomagnetic storms, earthquakes, volcanic eruptions, and sudden stratospheric warming SSW become the causes of variation in ionospheric electron density [1, 2]. A detailed investigation of these factors is required to understand the characteristics of the D-region ionosphere.

Low-frequency (LF, 30 kHz to 300 kHz) transmitter signals propagate with reflecting between the Earth's surface and the D-region ionosphere. When electron density in the D-region ionosphere changes, reflection height and propagation path change. Thus, the amplitude and phase of the received signal change. Therefore, by analyzing the received signal, it is possible to monitor variations in electron density along the propagation path.

So far, statistical comparisons between observation and the wave-hop method have not been performed. In this study, we investigate LT and seasonal variations in the D-region ionosphere using LF transmitter signals observed by the OCTAVE (Observation of CondiTion of ionized Atmosphere by VLF Experiment) network and compare the results of observation and wave-hop method.

Manuscript received 28 December 2022.

Yuma Nozaki, Hiroyo Ohya, and Hiroyuki Nakata is with Graduate School of Science and Engineering, Chiba University, 1-33 Yayoi-cho, Inage-ku, Chiba 263-8522, Japan; e-mail: yuuma201@chiba-u.jp, ohya@faculty.chiba-u.jp, nakata@faculty.chiba-u.jp.

Fuminori Tsuchiya is with Planetary Plasma and Atmospheric Research Center (PPARC), Graduate School of Science, Tohoku University, Aramaki-aza-aoba 6-3, Aoba, Sendai, Miyagi 980-8578, Japan; e-mail: tsuchiya@pparc.gp.tohoku.ac.jp.

Kenro Nozaki is with the University of Electro-Communications, 1-5-1 Chofugaoka, Chofu, Tokyo 182-8585, Japan; e-mail: kuboken@za2.so-net.ne.jp.

Kazuo Shiokawa is with the Institute for Space-Earth Environmental Research (ISEE), Nagoya University, Furo-cho, Chikusa-ku, Nagoya 464-8601 Japan; e-mail: shiokawa@isee.nagoya-u.ac.jp.

2. Observations

The transmitter and receiver used in this study were JJY (60 kHz, 33.47°N, 130.18°E) and RKB (Rikubetsu, 43.45°N, 143.77°E), respectively. The location of the path is shown in Figure 1. The observed data were amplitude and phase of the JJY–RKB path with 0.1-s sampling. For removing the effects of geomagnetic storms, we used five international quietest days for each month based on the Kp index determined by GeoForshungsZentrum Potsdam.

3. Results

Figure 2 shows the LT and seasonal dependence of the amplitude and phase variations of the LF transmitter signals in 2017. The daytime (or nighttime) mean values of amplitude and phase for each day (A_{mean} and P_{mean}) were subtracted from instantaneous values (A_i and P_i) to determine the perturbations in amplitude (ΔA) and phase (ΔP), that is, $\Delta A = A_i - A_{\mathrm{mean}}$ and $\Delta P = P_i - P_{\mathrm{mean}}$. The white lines indicate the time of sunrise/sunset at 70 km height. We regard the regions inside the white lines as daytime data for Figures 2a and

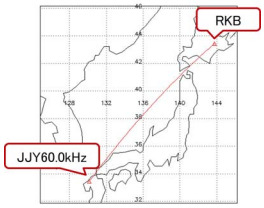

Figure 1. Location of the JJY-RKB path.

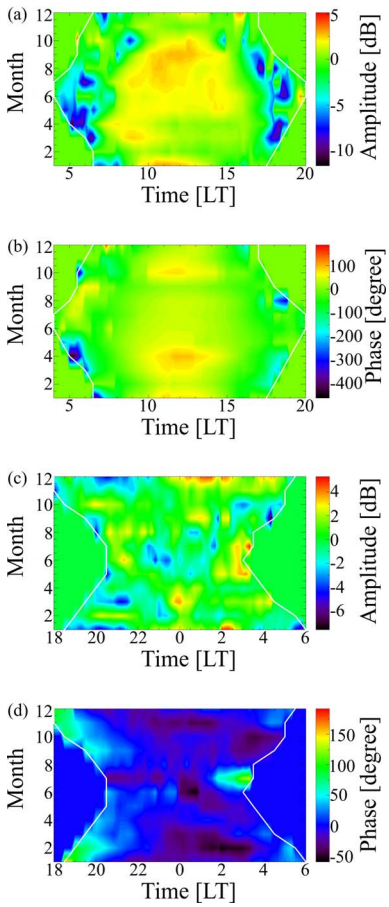

Figure 2. (a) Observed ΔA in daytime, (b) observed ΔP in daytime, (c) observed ΔA in nighttime, and (d) observed ΔP in nighttime.

2b and nighttime data for Figures 2c and 2d. In daytime, as shown in Figures 2a and 2b, both ΔA and ΔP from 09:00 LT to 15:00 LT were larger than those at the other LT. For seasonal variations, ΔA was large in summer and winter, while ΔP was large in spring and fall. Both ΔA and ΔP were large in January.

In nighttime, as shown in Figures 2c and 2d, ΔA has no clear dependences on both LT and season, while the ΔP was large around sunset/sunrise.

4. Comparison Between Observations and Calculations

The observed results were compared with the calculated results based on the wave-hop method. The wave-hop method calculates the resultant field strength by adding the fields of the ground wave and K-hop sky waves ($K = 1, 2, 3, \cdots and 10$) [3, 4] (Figure 3). The frequency of the LF transmitter (60 kHz) used in this study is within the application range of the wave-hop method. In the case of short paths (1000 km to 2000 km), results of the long wavelength propagation capability (LWPC) for very low frequency (VLF) waves (15 kHz) match those of the wave-hop method [5]. The wave-hop method can be easily understood and

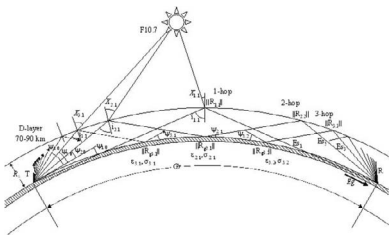

Figure 3. Geometry of the wave-hop method [3].

is a more useful for calculation of VLF/LF waves than LWPC/finite-difference time domain. The resultant electric field strength E was calculated as follows:

$$E = Eg + \sum_{K=1}^{10} Es_K \tag{1}$$

where K is the number of hops, Eg is the ground wave, and Es_K is the effective field strength of transmitted sky waves. The electric field strength of ground wave Eg was calculated as follows:

$$Eg = |Eg| \exp(jkG_r) \tag{2}$$

where k is the wave number of the LF signals, G_r is the great circle distance between the transmitter and receiver, and $|Eg|$ was calculated based on [6]. The electric field strength of K-hop sky waves Es_K was calculated for a loop antenna as follows:

$$Es_K = \frac{600\sqrt{Pt}\cos\psi \prod_{L=1}^{K}(Rc_{K,L})}{\sum_{L=1}^{K}(Pl_{K,L})} \times \prod_{L=1}^{K-1}(Rg_{K,L}) Fc_K Ft_K Fr_K \exp\left(-jk\sum_{L=1}^{K} Pl_{K,L}\right) \tag{3}$$

where Pt (=22.5 kW) is the radiated power (kW), ψ (=0.046 rad in the case of a one-hop wave; reflection height = 90 km) is the angle of departure and arrival of the sky wave at the ground, L is the number of reflection points from the transmitter, Rc is ionospheric reflection coefficient, Rg ($\simeq$1.0) is the reflection coefficient of the Earth's surface, Fc is the ionospheric focusing factor, Ft is the transmitting antenna factor, Fr is the receiving antenna factor, and Pl (=1619.1 km in the case of a one-hop sky wave; reflection height = 90 km) is the path length of each sky wave, and L is apex number from 1 to K. For example, in the case of a three-hop sky wave, the hop point near the transmitter is L=1, the middle hop point is $L = 2$, and the hop point near the receiver is $L = 3$. Rc is determined by an empirical value that depends on the solar zenith angle and the frequency of the transmitter [3]. Fc is also determined by [3] and depends on the horizontal distance between the transmitter and receiver and daytime/nighttime. Ft and Fr are determined by Earth's surface (land, sea, or ice), frequency of transmitter, and elevation angle according to [3]. We used electron density-height profiles of the International Reference Ionosphere (IRI) 2016 model. We determined the height where the frequency of the transmitter (60 kHz) is equal to the electron plasma

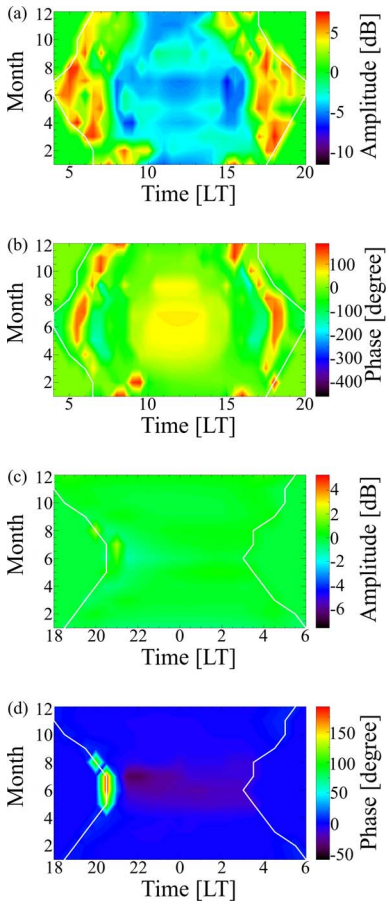

Figure 4. (a) Calculated ΔA in daytime, (b) calculated ΔP in daytime, (c) calculated ΔA in nighttime, (d) calculated ΔP in nighttime.

frequency as the reflection height. The path length *Pl* of each sky wave in (3) is calculated geometrically.

Figure 4 shows the calculation results of ΔA and ΔP in daytime and nighttime based on the wave-hop method. In the daytime, as shown in Figures 2a and 4a, an increase/decrease of observed ΔA was opposite of the calculated one. Comparing daytime ΔP (Figures 2b and 4b), large ΔP observed in summer is similar to the calculated one, although the observed ΔP at sunrise/sunset is different from the calculated one. As for seasonal variation, the calculated ΔP showed a large depression in the summer.

In nighttime, as shown in Figures 2c, 2d, 4c, and 4d, there were almost no variations in calculation results, although observed data showed temporal variations in ΔA and ΔP.

We considered the cause of the difference between observations and calculations as follows: 1) the assumed reflection height for calculation was different from the actual one, and 2) disturbances due to neutral winds (e.g., planetary waves, gravity waves, acoustic waves) were not included in the calculation.

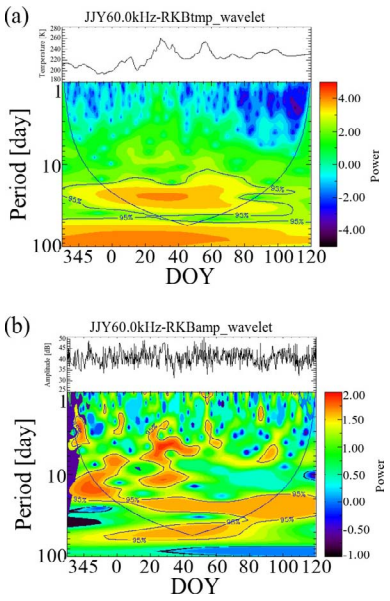

Figure 5. Wavelet spectra of (a) stratospheric temperature and (b) LF amplitude.

5. Discussion: SSW Effects

In Figure 2, both ΔA and ΔP were large in January 2017, which was not expected from the wave-hop method and the IRI-2016 model. We investigated the relationship between large LF amplitude in January 2017 and SSW. We calculated mean temperature at 10 hPa, where the latitude and longitude were >60°N and 110°E to 170°E, respectively, based on the Japanese 55-year reanalysis (JRA-55) data set. The previous study showed that the SSW around January 29, 2017, was a major warming, as the temperature at 10 hPa (∼31 km height) increased by 38 K [7].

Figure 5 shows the wavelet spectra of 1) the mean temperature and 2) the LF amplitude from December 1, 2016, to April 30, 2017. The *x*-axis indicates day of year. Figure 6 shows coherence between the stratospheric temperature and the LF amplitude. As shown in Figures 5a and 5b, both the stratospheric temperature and the LF amplitude had two periods of 5 days and 21 days. Figure 6 shows a coherence between the temperature and LF amplitude. The coherence for periods of 5 days and 21 days was high, at 0.55 and

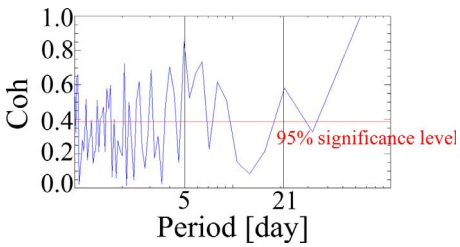

Figure 6. Coherence between stratospheric temperature and LF amplitude.

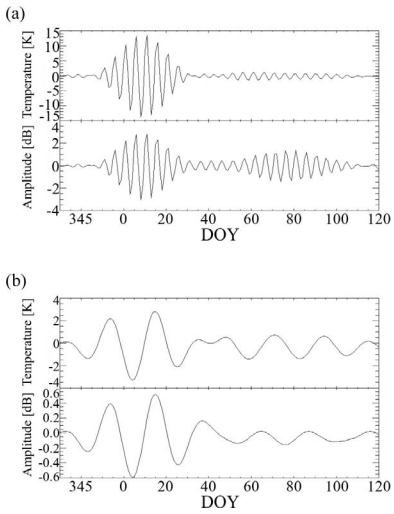

Figure 7. Band-pass–filtered waveforms of (upper) temperature and (lower) LF amplitude. (a) five-day period; (b) 21-day period.

0.86, respectively, which were over the 95% significance level.

Figure 7 shows band-pass–filtered waveforms of (upper) temperature and (lower) LF amplitude. Figures 7a and 7b show periods for five days (band-pass filter: 4.5 days to 5.5 days) and 21 days (band-pass filter: 20.5 days to 21.5 days), respectively. As shown in Figure 7, the LF amplitude and temperature were almost in phase within the time resolution of 24 h.

This suggests that an increase in stratospheric temperature at high latitudes may be associated with LF amplitude at the midlatitudes via neutral winds.

During the SSW, the LF amplitude was large and had similar periods with the temperature at high latitudes. In previous studies for the same 2017 SSW, two-day waves were observed by meteor radar in China (19.0°N, 109.8°E), and planetary waves were enhanced [7]. This study suggests that SSW affects the D-region ionosphere at midlatitudes via neutral winds.

6. Conclusions

We investigated LT and seasonal variations in the D-region ionosphere using LF transmitter signals of the JJYRKB path over Japan in 2017. The SSW effects on the LF amplitude in January 2017 were investigated.

Both ΔA and ΔP were large from 9:00 LT to 15:00 LT. ΔA variations were large in summer and winter, while ΔP variations were large in spring and fall. There were small variations in the LF amplitude and phase in nighttime in spite of no variations calculated from wave-hop method and the IRI-2016 model. An increase/decrease of daytime observation ΔA showed the opposite to calculation results based on wave-hop method. However, observed ΔP variations were similar with the calculated one. The differences of ΔA and ΔP between observations and calculations were caused by the actual reflection height and ionospheric disturbances that are not included in the IRI-2016 model.

Both ΔA and ΔP were large in January 2017. There were similar periods of five days and 21 days both in stratospheric temperature at high latitudes and in LF amplitudes at midlatitudes. The temperature and LF amplitude were in phase with a time resolution of 24 h. This suggests that the SSW may affect the LF propagation at midlatitudes via neutral winds.

7. Acknowledgment

The JRA-55 data sets were provided by the Japan Meteorological Agency.

8. References

1. S. Pal, Y. Hobara, S. K. Chakrabarti, and P. W. Schnoor, “Effects of the Major Sudden Stratospheric Warming Event of 2009 on the Subionospheric Very Low Frequency/Low Frequency Radio Signals,” *Journal of Geophysical Research: Space Physics*, **122**, 7, June 2017, pp. 7555-7566.
2. J. Laštovička, “Forcing of the Ionosphere by Waves From Below,” *Journal of Atmospheric and Solar-Terrestrial Physics*, **68**, 3-5, February 2006, pp. 479-497.
3. International Telecommunication Union, “Recommendation ITU-R P.684-7, Prediction of Field Strength at Frequencies Below 150 kHz,” October 2016.
4. H. Ohya, F. Tsuchiya, Y. Takishita, H. Shinagawa, K. Nozaki, and K. Shiokawa, “Periodic Oscillations in the D Region Ionosphere After the 2011 Tohoku Earthquake Using LF Standard Radio Waves,” *Journal of Geophysical Research: Space Physics*, **123**, 6, June 2018, pp. 5261-5270.
5. S. Tsuciya, K. Imamura, H. Ito, H. Maeno, M. Kubota, and K. Nozaki, “Prediction Method and Proof Measurement of LF Standard Frequency Waves,” *Seasonal Report of National Institute of Information and Communication Technology*, **56**, September 2010, pp. 97-108.
6. International Telecommunication Union, “Recommendation ITU-R P.368-7, Ground-Wave Propagation Curves for Frequencies Between 10 kHz and 30 MHz,” March 1992.
7. J. Xiong, W. Wan, F. Ding, L. Liu, L. Hu, and C. Yan, “Two Day Wave Traveling Westward With Wave Number 1 During the Sudden Stratospheric Warming in January 2017,” *Journal of Geophysical Research: Space Physics*, **123**, 4, March 2018, pp. 3005-3013.